

Improving range of SPR tunability and extinction efficiency of spheroidal silver nanostructures in graphene environment

SHIVANI BHARDWAJ* and R P SHARMA

Centre for Energy Studies, IIT Delhi, New Delhi 110016, India

*Author for correspondence (sshivanni@gmail.com)

MS received 20 March 2018; accepted 28 May 2018; published online 3 September 2018

Abstract. In photovoltaics, the materials having ability to manipulate the optical fields and coupling of energy flow inside the device play a crucial role. In this article, we report the role of graphene environment on spheroid-shaped Ag nanoparticles (NPs) with various shapes and sizes. This study confirms the tunability of surface plasmon resonances (SPRs) and an enhancement in extinction efficiency, derived numerically using discrete dipole approximation (DDA). We have chosen oblate- and prolate-shaped Ag NPs for the numerical experiment and analysed their optical signatures in terms of extinction efficiency and SPR tunability against the quasi-static approximation. The excitation of longitudinal and transversal resonances was also observed because of the asymmetric shape of Ag NPs. All optical responses have been analysed by varying the effective radii and aspect ratio of Ag NPs, and the thickness of graphene monolayer (from 0.1 to 0.5 nm). Tunability of longitudinal resonances has been observed in the 600–833 nm wavelength region, while for transversal resonances, the tunability is in the 450–505 nm wavelength range. The results represent the effect of graphene environment on the tunability of SPRs with enhanced extinction efficiency. This study could lead to the development of a photovoltaic device with wide range of tunability and enhanced efficiency.

Keywords. Discrete dipole approximation; graphene–plasmon interaction; spheroid-shaped Ag NPs; extinction efficiency; graphene monolayer surrounding environment; localized surface plasmon resonances.

1. Introduction

Ultra-thin devices and nanostructures are needed to enhance light–matter interaction, lessen the material usage and also allow more efficient charge collection to deal with a next-generation photovoltaic device [1–3]. Due to the reduction in optical thickness of the absorber material in such devices, electromagnetic devices such as nano-optic cavities, localized surface plasmons (LSPs) and photonic crystals have been introduced to enhance the absorption mechanism, which leads to higher photocurrent conversion process [1,4,5]. Metal nano-particles (MNPs) that strongly support LSPs are widely utilized in different fields of applications such as ultrafast optical switching [6], biological sensors [6], optical data storage [7], optical tweezers [8], light-emitting diodes [9], surface-enhanced Raman scattering [10], solar energy conversion [1], etc. Tunability of the plasmonic modes for MNPs highly depends on their shape, size, physical environment, variation of the dielectric functions and one-to-one interaction of the nanoparticles (NPs) [11–13]. Among them, asymmetric-shape MNPs have two or three different orthogonal principal axes that possess multiple plasmonic modes due to their large degree of freedom for the coherent excitation of the conductive electrons oscillating along each axis. The longitudinal (along major axis) and transversal (along minor axis) plasmonic resonances are excited by the charge accumulation

of oscillating electrons along the respective axes of NPs [14,15]. The coupling between the longitudinal and transversal plasmonic modes of the MNPs plays an important role in enhancing the resonant broadband absorption inside the active layer. In previous studies one can observe that the surface plasmon resonance (SPR) tunability of the MNPs is not appropriate, with a limited wavelength range of tunability [15,16]. Hence, there is a strong need of an advance material with its unique optical properties that lead to a wide range of SPR tunability for NPs from visible to IR domain. To increase the efficiency of the photovoltaic devices, many of the researchers have used different surrounding environments of MNPs. Nowadays, graphene monolayer (GML) is widely used as a spacer, substrate, coating material and surrounding environment in the solar cell devices due to its fascinating optical and electrical properties [17–20].

Graphene is a flexible, ultimate-thin 2D material that supports its own plasmonic properties. Graphene plasmonics is a unique and attractive field that gives a new generating platform to promote strong light–matter interaction that enables extreme light confinement. The unusual optical properties of graphene depend on its transparency, conductivity, flexibility and strength, which are extremely high and stable at room temperature [19–22]. Due to such fascinating behaviour, graphene shows outstanding optical features that promote tuning over a wide range of SPR in AM1.5 Spectra.

The optical and electrical properties of graphene are frequently used in photovoltaics to enhance the photon current density of the solar cells.

In this article, we have studied the interaction between spheroid-shaped silver NPs and GML by the DDA technique. Here we have chosen three different types of spheroidal Ag NPs: sphere, oblate and prolate, to identify the significant enhancement in their extinction efficiencies (Q_{ext}) and the SPR tunability. The ASR of the proposed nano-geometries is varied from 0.3 to 0.9. Thickness of surrounding environment of the MNPs $t_{\text{GML}} = 0.1$ nm has been considered for the proposed nano-geometries to achieve the optical broadband SPR tunability that covers visible to near-IR domain. Modified optical parameters of the silver NPs have been taken from the literature [23,24].

2. Theory

2.1 Computational method

Discrete dipole approximation (DDA) is one of the most powerful and flexible electro-dynamics numerical techniques that describes optical signatures such as absorption, scattering and extinction efficiency with excellent accuracy of the entire volume for targets of any arbitrary geometry [25–27].

In DDA, the target geometry is treated as an array of N points of dipoles. The location (\vec{r}_i), and polarizability ($\vec{\alpha}_i$) of the N -point dipoles are the essential parameters for the DDA simulations [12,25,26]. The dipole moment of the target geometry is expressed as

$$\vec{p}_i = \alpha_i \cdot \vec{E}_{i,\text{loc}} \quad (1)$$

$$\vec{E}_{i,\text{loc}} = \vec{E}_{i,\text{app}} + \vec{E}_{i,\text{ind}} \quad (2)$$

$$\vec{E}_{i,\text{app}} = E_0 e^{i(\vec{k} \cdot \vec{r} - \omega t)} \quad (3)$$

$$\vec{E}_{i,\text{ind}} = - \sum_{j=1}^N \vec{A}_{ij} \cdot \vec{p}_j \quad (4)$$

where \vec{k} represents the incident wave vector.

$\vec{E}_{i,\text{loc}}$ is the local electric field established by the applied electromagnetic field $\vec{E}_{i,\text{app}}$ on the array of point dipoles. $\vec{E}_{i,\text{ind}}$ is the induced electric field produced by the radiation of all others $N-1$ dipoles acting on the i th individual point dipole. The A_{ij} with $i \neq j$ is an interaction matrix with 3×3 matrices as elements, such that [25,27,28]

$$\vec{A}_{ij} \cdot \vec{p}_j = \frac{e^{ikr_{ij}}}{r_{ij}^3} \left\{ k^2 \vec{r}_{ij} (\vec{r}_{ij} \times \vec{p}_j) + \frac{(1 - ikr_{ij})}{r_{ij}^2} \times \left[r_{ij}^2 \vec{p}_j - 3\vec{r}_{ij} (\vec{r}_{ij} \cdot \vec{p}_j) \right] \right\} \quad (5)$$

and

$$\vec{p}_i = \alpha_i \cdot \left(\vec{E}_{i,\text{app}} - \sum_{j=1}^N \vec{A}_{ij} \cdot \vec{p}_j \right) \quad (6)$$

where $r_{ij} = |\vec{r}_j - \vec{r}_i|$ and $\vec{r}_{ij} = \vec{r}_i - \vec{r}_j$. Once we know each p_i of the target geometry, it is possible to calculate the extinction, absorption and scattering cross-sections using the following expressions [25,29]:

$$C_{\text{ext}} = \frac{4\pi k}{|\vec{E}_0|^2} \sum_{i=1}^N \text{Im} \left\{ \vec{E}_{i,\text{inc}}^* \cdot \vec{p}_i \right\} \quad (7)$$

$$C_{\text{abs}} = \frac{4\pi k}{|\vec{E}_0|^2} \sum_{i=1}^N \left\{ \text{Im} \left[\vec{p}_i \cdot (\alpha_i^{-1})^* \vec{p}_i \right] - \frac{2}{3} k^3 |\vec{p}_i|^2 \right\} \quad (8)$$

$$C_{\text{sca}} = C_{\text{ext}} - C_{\text{abs}} \quad (9)$$

$$Q_l = \frac{C_l}{\pi a_{\text{eff}}^2} \quad (10)$$

where C_l is the optical cross-sectional area of the target geometry and l is the running index of optical cross-sectional area (scattering, absorption and extinction) of the point dipole. Q_l is the normalized optical cross-section and a_{eff} is the effective radius of target geometry.

2.2 Optical response of graphene

The optical responses of the graphene are described using the Kubo formula in terms of the surface conductivity [25,30,31]. The frequency-dependent complex-valued surface conductivity of graphene depends on its intra-conductivity σ_{intra} and inter-conductivity σ_{inter} . The dynamic surface conductivity can be quantitatively described as [17,18,21]

$$\sigma_{2D}(\omega) = \sigma_{\text{intra}}(\omega, \mu_c, \Gamma, T) + \sigma_{\text{inter}}(\omega, \mu_c, \Gamma, T) \quad (11a)$$

$$\sigma_{\text{intra}}(\omega, \mu_c, \Gamma, T) = -i \frac{e^2 k_B T}{\pi \hbar^2 (\omega - i2\Gamma)} \times \left[\frac{\mu_c}{k_B T} + 2 \ln \left(\exp \left(-\frac{\mu_c}{k_B T} \right) + 1 \right) \right] \quad (11b)$$

$$\sigma_{\text{inter}}(\omega, \mu_c, \Gamma, T) = -i \frac{e^2}{4\pi \hbar} \times \ln \left[\frac{2|\mu_c| - \hbar(\omega - i2\Gamma)}{2|\mu_c| + \hbar(\omega - i2\Gamma)} \right] \quad (11c)$$

where ω is the frequency of the incident light, Γ is relaxation process rate having $\Gamma \leq 1$ meV, μ_c is the chemical potential of graphene that lies in approximately 50–1000 meV range and

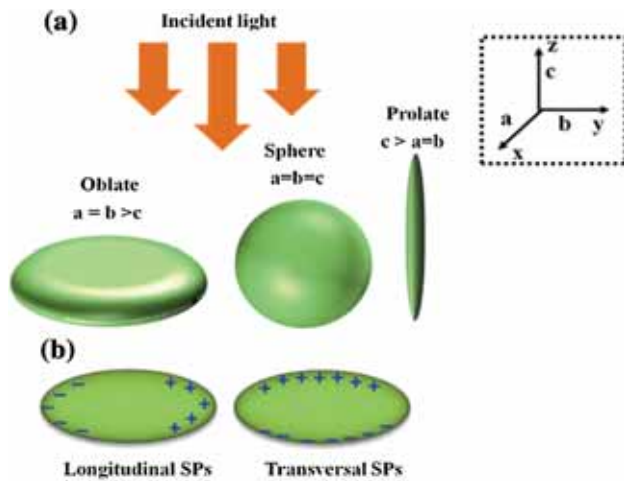


Figure 1. Schematic diagram of (a) 3D spheroid-shaped Ag NPs surrounded by the graphene monolayer (GML) environment, having the dielectric function $\varepsilon(\omega)$. (b) Generalized presentation of charge accumulation for longitudinal and transversal surface plasmons in oblate-shaped Ag NPs.

\hbar is reduced Planck's constant. Further, relative permittivity of graphene $\varepsilon_g(\omega)$ can be obtained by coupling of Ohm's law and Maxwell's equation, which is proportional to its complex-valued surface conductivity as follows [18,30]:

$$\varepsilon_g(\omega) = \left(\varepsilon_0 + i \frac{\sigma_{2D}(\omega)}{\omega t} \right), \quad (12)$$

where ε_0 is the permittivity of free space and t is the thickness of GML.

A schematic diagram of the spheroid-shaped: oblate ($a = b > c$), spherical ($a = b = c$) and prolate ($c > a = b$), Ag NPs is shown in figure 1a. Figure 1b shows the charge accumulation on the surface of the oblate-shaped Ag NP in two different modes of polarization. The charge accumulation highly depends on the shape of the NP. If the charge accumulations are excited along the major axis they are called longitudinal plasmons, while along the minor axis they are known as transversal plasmons. The longitudinal and transversal plasmons lie in the higher and lower wavelength region, respectively, due to the restoring force, which is proportional to the strength of the charge accumulation [32].

3. Results and discussion

Plasmon coupling between the Ag NPs and GML surrounding environment provides the guided information to understand basic phenomena of the enhancement in extinction efficiency and the SPR tunability of the Ag NPs embedded in the surrounding medium of graphene. This amplified efficiency plays a significant role in harvesting the absolute light trapping due to the increased effective path length of the incident

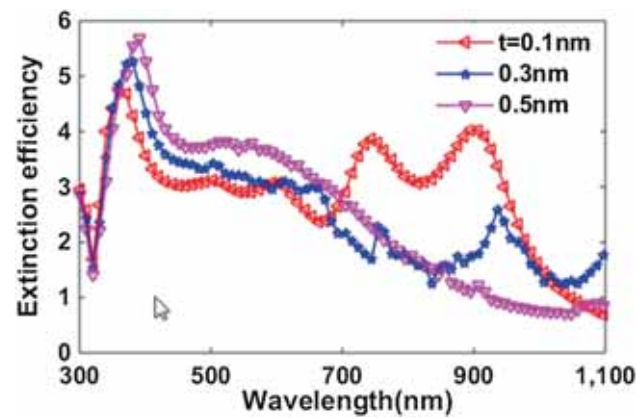


Figure 2. Extinction efficiency Q_{ext} of spherical Ag NPs at fixed effective radius $a_{\text{eff}} = 100$ nm with GML of three different thicknesses ($t = 0.1, 0.3$ and 0.5 nm) as the surrounding environment.

light, which is responsible for improving the absorption of photons inside ultra-thin silicon substrate.

Figure 2 helps us to understand the modification in the extinction efficiency of sphere-shaped Ag NPs embedded in homogeneous surrounding environments of graphene. Extinction efficiency of Ag NPs has been calculated using equation (10). We have chosen a fixed effective radius ($a_{\text{eff}} = 100$ nm) of the spherical Ag NP to show remarkable resonance effect with different thicknesses of graphene (t_{GML}) as the host medium. For $t_{\text{GML}} = 0.1$ nm, there is the existence of the multiple plasmonic peaks in the lower as well as higher wavelength region simultaneously, which covers the resonant broadband spectrum (extinction efficiency lies in UV-IR domain) other than two thicknesses (0.3 and 0.5 nm) of GML as shown in figure 2. Therefore, $t_{\text{GML}} = 0.1$ nm of surrounding environment has been considered for further analysis.

In the further discussion, asymmetric-shape NPs (oblate and prolate) have been introduced to analyse the variation in SPR tunability and extinction efficiency compared with symmetrical (spherical-shaped) NPs. The multiple peaks in SPR spectra of asymmetric NPs are observed because of the displacement of the electron cloud, which is non-homogenous about all axes while it is homogeneous for symmetrical NPs.

Figure 3 shows the wavelength-dependent extinction efficiency spectra of oblate ($a = b > c$) Ag NPs embedded in graphene environment. Figure 3a–c presents the resonant broadband of the extinction efficiency spectrum of oblate-shaped Ag NPs for different ASR = 0.3, 0.5 and 0.9, respectively, where a_{eff} of the Ag NPs has been varied from 60 to 100 nm. For oblate-shaped Ag NPs, there is two-fold symmetry and hence, two pronounced peaks occur; one lies in higher wavelength regime at $\lambda_{\text{SPR}} = 820.8$ nm corresponding to major axis (longitudinal axis) and other lies in the lower wavelength limit at $\lambda_{\text{SPR}} = 600$ nm corresponding to minor axis (transverse axis), in the broad

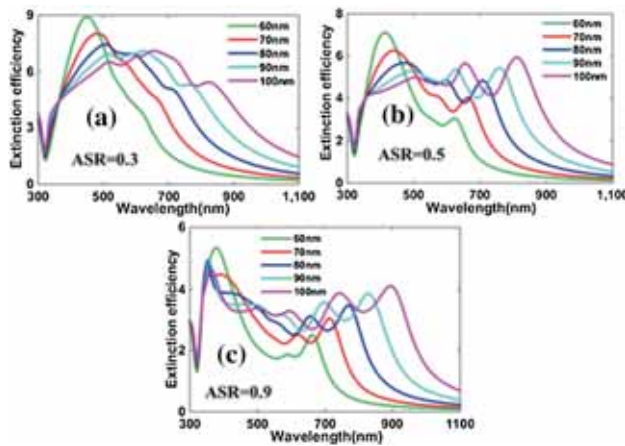


Figure 3. Extinction efficiency Q_{ext} as a function of wavelength for the oblate-shaped Ag NPs for three different ASRs: (a) 0.3, (b) 0.5 and (c) 0.9, with five different effective radii of 60, 70, 80, 90 and 100 nm embedded in GML environment.

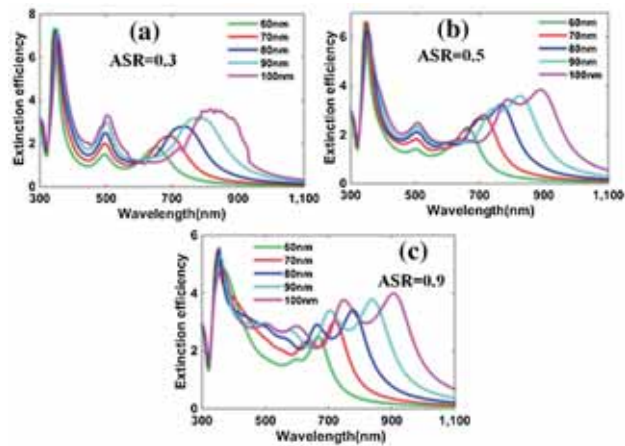


Figure 4. Extinction efficiency Q_{ext} as a function of wavelength for the prolate-shaped Ag NPs for three different ASRs: (a) 0.3, (b) 0.5 and (c) 0.9, with five different effective radii of 60, 70, 80, 90 and 100 nm embedded in GML environment.

resonant spectra of Q_{ext} at $a_{\text{eff}} = 100$ nm and $\text{ASR} = 0.3$. For oblate-shaped Ag NPs the resonant peaks lying in the higher wavelength region are more tunable at $\text{ASR} = 0.3$, having the magnitude of the extinction efficiency 4.146 ($\lambda_{\text{SPR}} = 600$ nm), 4.554 ($\lambda_{\text{SPR}} = 665$ nm), 5.045 ($\lambda_{\text{SPR}} = 713.4$ nm), 5.353 ($\lambda_{\text{SPR}} = 772.5$ nm) and 5.442 ($\lambda_{\text{SPR}} = 820.8$ nm) as the effective radius increases from minimum to maximum (60–100 nm) value. Thus, it is observed that the highly tunable resonant peaks lying in the optical broadband of Q_{ext} spectrum get red-shifted as a_{eff} increases up to 100 nm while there is a blue shift in SPR peak as the ASR increases from 0.3 to 0.9.

Figure 4 illustrates the variation of extinction efficiency with the wavelength of the incident light for prolate-shaped

Ag NPs, by changing the ASR and effective radii of the NPs in the host medium of graphene. The prolate-shaped Ag NPs also show similar features as those of oblate-shaped Ag NPs (as shown in figure 3) with lower magnitude of optical broadband extinction efficiency Q_{ext} . From figure 4a, it can be observed that the plasmonic peak lies in higher wavelength (649–833 nm, approximately) domain having the magnitude of the extinction efficiencies as 1.847 ($\lambda_{\text{SPR}} = 649$ nm), 2.259 ($\lambda_{\text{SPR}} = 686.6$ nm), 2.787 ($\lambda_{\text{SPR}} = 729.5$ nm), 3.192 ($\lambda_{\text{SPR}} = 778$ nm) and 3.58 ($\lambda_{\text{SPR}} = 833$ nm) at fixed $\text{ASR} = 0.3$ with variation in a_{eff} from 60 to 100 nm. These SPR peaks are red-shifted as the a_{eff} increases from 60 to 100 nm with tunability of 184 nm, approximately. Further, we can see that the magnitude of these tunable resonant peaks (lies in the higher wavelength limits) gradually increases with increase in ASR as shown in figure 4a–c. There is a blue-shift in extinction efficiency spectrum with increase in ASR because it approaches towards spherical geometry as ASR increases to its maximum value as shown in figure 4a–c.

Here, we have analysed that as the ASR increases from 0.3 to 0.9, the individual effects of the longitudinal and the transversal resonances merge together, giving rise to the broadband spectrum of extinction efficiency. This happens because of excitation of the free electron density oscillations becoming homogenous on the surface of NPs due to the increment in ASR and ideally approaches the extinction efficiency spectra of sphere as discussed earlier (figure 1).

4. Conclusion

In the present study, we have used DDA to study the extinction efficiency and SPR tunability of Ag NPs of different sizes and shapes, surrounded in a graphene environment. Here, we have considered the oblate and prolate shapes of Ag NPs against the quasi-static approximation, where the effective radii of the Ag NPs are greater than 50 nm (varies from 60 to 100 nm). It has been observed that high tunable longitudinal plasmonic resonances for both asymmetric (oblate and prolate)-shaped Ag NPs are red-shifted as the a_{eff} increases from 60 to 100 nm. In case of the oblate-shaped Ag NPs, the tunabilities of longitudinal and transverse plasmonic resonance are approximately 220 and 69 nm, respectively; on the other hand, for the prolate shape they are approximately 184 and 12 nm, respectively, as a_{eff} increases up to its maximum limit (100 nm). The proposed metal nano-geometries (oblate and prolate) in graphene environment can be effectively used to trap incident light in the sub-wavelength regime as a requirement of the scientific community.

Acknowledgement

One of the authors (Shivani Bhardwaj) is thankful to MNRE, India, for providing the financial support for this research.

References

- [1] Atwater H A and Polman A 2010 *Nat. Mater.* **9** 205
- [2] Catchpole K R and Polman A 2008 *Appl. Phys. Lett.* **93** 191113
- [3] Nakayama K, Tanabe K and Atwater H A 2008 *Appl. Phys. Lett.* **93** 121904
- [4] Kim S K *et al.* 2014 *ACS Nano* **8** 3707
- [5] Bermel P, Luo C, Zeng L, Kimerling L C and Joannopoulos J D 2007 *Opt. Express* **15** 16986
- [6] Hideyuki I, Koichiro T, Ichiro T, Toshiaki H and Hiroki N 2000 *Jpn. J. Appl. Phys.* **39** 5132
- [7] Ditlbacher H, Krenn J R, Lamprecht B, Leitner A and Aussenegg F R 2000 *Opt. Lett.* **25** 563
- [8] Juan M L, Righini M and Quidant R 2011 *Nat. Photon.* **5** 349
- [9] Liang Z, Sun J, Jiang Y, Jiang L and Chen X 2014 *Plasmonics* **9** 859
- [10] Nie S and Emory S R 1997 *Science* **275** 1102
- [11] Noguez C 2007 *J. Phys. Chem. C* **111** 3806
- [12] Amendola V, Bakr O M and Stellacci F 2010 *Plasmonics* **5** 85
- [13] Kelly K L, Coronado E, Zhao L L and Schatz G C 2003 *J. Phys. Chem. B* **107** 668
- [14] Koppens F H L, Chang D E and García de Abajo F J 2011 *Nano Lett.* **11** 3370
- [15] Alsawafat M, Wahbeh M and Truong V V 2012 *J. Nano-mater.* **2012** 10
- [16] Grand J *et al.* 2006 *Plasmonics* **1** 135
- [17] Bhardwaj S, Pathak N K, Ji A, Uma R and Sharma R P 2017 *Plasmonics* **12** 193
- [18] Bhardwaj S, Uma R and Sharma R P 2016 *Plasmonics* **12** 961
- [19] Grigorenko A N, Polini M and Novoselov K S 2012 *Nat. Photon.* **6** 749
- [20] Jablan M, Soljačić M and Buljan H 2013 *Proc. IEEE* **101** 1689
- [21] Lu H, Cumming B P and Gu M 2015 *Opt. Lett.* **40** 3647
- [22] Novoselov K S *et al.* 2005 *Nature* **438** 197
- [23] Palik E D 1998 *Handbook of optical constants of solids* (San Diego: Academic)
- [24] Johnson P B and Christy R W 1972 *Phys. Rev. B* **6** 4370
- [25] Sosa I O, Noguez C and Barrera R G 2003 *J. Phys. Chem. B* **107** 6269
- [26] Draine B T and Flatau P J 2008 *J. Opt. Soc. Am. A* **25** 2693
- [27] Draine B T and Flatau P J 2013 *ArXiv preprint* arXiv:1305.6497
- [28] Draine B T and Flatau P J 1994 *J. Opt. Soc. Am. A* **11** 1491
- [29] Bohren C F and Huffman D R 2008 *Absorption and scattering of light by small particles* (Weinheim, Germany: John Wiley & Sons)
- [30] Zhao B, Zhao J M and Zhang Z M 2014 *Appl. Phys. Lett.* **105** 031905
- [31] Wang B, Zhang X, Yuan X and Teng J 2012 *Appl. Phys. Lett.* **100** 131111
- [32] García M A 2011 *J. Phys. D: Appl. Phys.* **44** 283001